Supporting Information

Interfacial In-S_V-N bond mediated d/p-band center up-shift in a S-scheme heterojunction for boosting photocatalytic H_2 evolution

Xue Jiang,[a] Sheng Guo,[a] Chaofan Yuan,[a] Na Tian,[*,a] Ning Zhang,[b] Qian Zhang,[b] Fang Chen,[a] Yihe Zhang,[a] Hongwei Huang[*,a]

[a] Engineering Research Center of Ministry of Education for Geological Carbon Storage and Low Carbon Utilization of Resources, Beijing Key Laboratory of Materials Utilization of Nonmetallic Minerals and Solid Wastes, National Laboratory of Mineral Materials, Hebei Key Laboratory of Resource Low-carbon Utilization and New Materials, School of Materials Science and Technology, China University of Geosciences (Beijing), 100083, China

[b] School of Resources and Environmental Engineering, Shandong University of Technology, 255049 Zibo, PR China

*Corresponding author: tianna65@cugb.edu.cn (N. Tian); hhw@cugb.edu.cn (H.W. Huang)

Table of Contents

Results and Discussion

1.XRD, FT-IR, SEM and EDS elemental mapping images of as-synthesized catalysts

FT-IR spectra (Fig. S1b) reveal a pronounced hydroxyl peak at 3000-3600 cm^{-1} for S_V-ZIS and S_V-ZIS/CN, which is absent in pristine ZIS and ZIS/5CN. This indicates that introducing S-vacancies promotes surface hydroxyl adsorption, forming a protective layer that enhances photostability by inhibiting ZIS self-degradation. Furthermore, the spectrum of S_V-ZIS/CN exhibits characteristic peaks of both CN and S_V-ZIS, corroborating its successful synthesis[1,2].

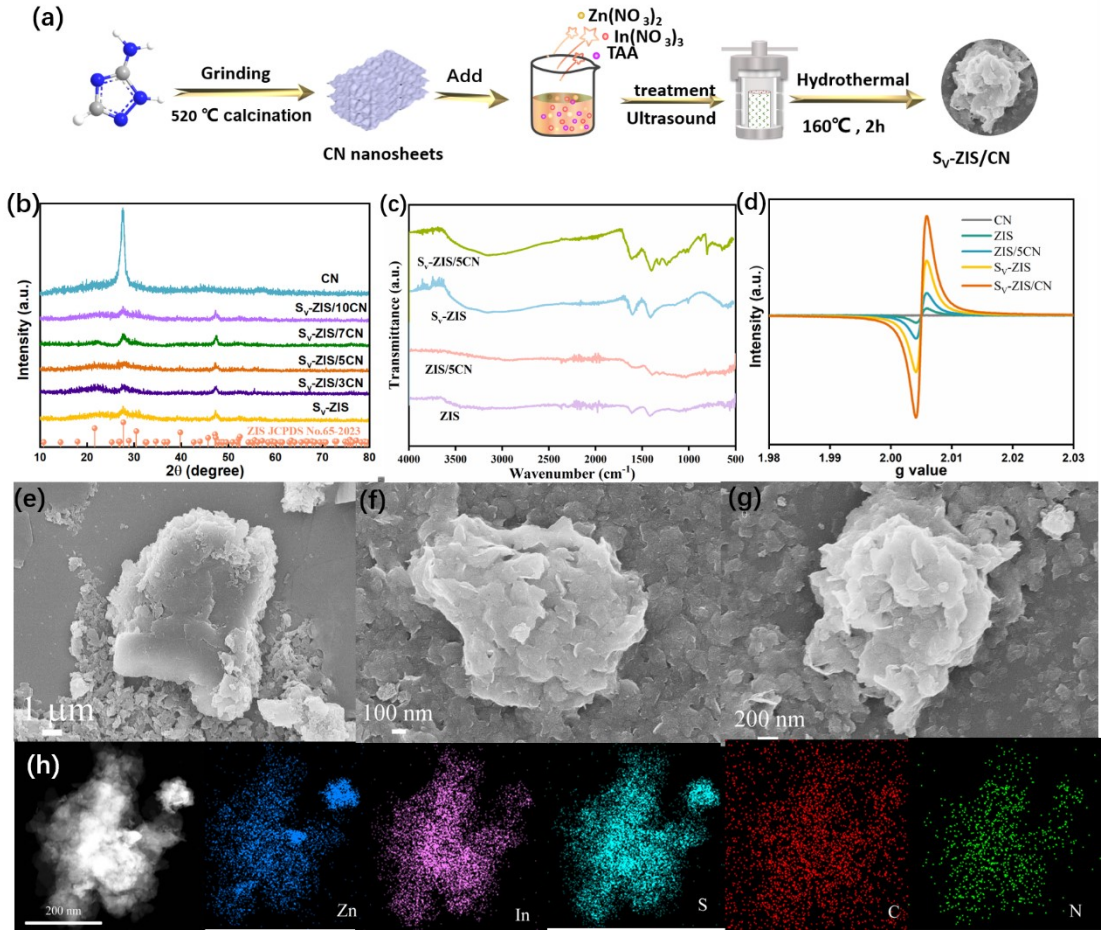

Fig. S1 (a) Scheme illustration of S_V-ZIS/CN heterojunction, (b) XRD patterns, (c) FTIR results of ZIS, ZIS/5CN, S_V-ZIS and S_V-ZIS/5CN heterojunction, (d) Quantitative EPR test of samples, SEM images of (e) CN, (f) S_V-ZIS and (g) S_V-ZIS/5CN and EDS elements mapping images (h) of S_V-ZIS/5CN heterojunction.

2. N_2 adsorption–desorption isotherms and pore size distributions results of as-synthesized catalysts

The nitrogen adsorption–desorption curve can more clearly show the changes in specific surface area and porosity. The nitrogen adsorption-desorption isotherms (Fig. S2a) showed a typical IV-type isotherm, and the Barrett-Joyner-Hall (BJH) pore size distribution curve (Fig. S2b) indicated that the samples had mesoporous characteristics[3,4]. Compared with ZIS (105.69 m^2 g^{-1}) and ZIS/CN (95.63 m^2 g^{-1}), the specific surface areas of S_V-ZIS and S_V-ZIS/5CN samples after introducing S vacancies were both increased, reaching 118.30 m^2 g^{-1} and 101.02 m^2 g^{-1}, which were higher than that of the CN (5.32 m^2 g^{-1}).

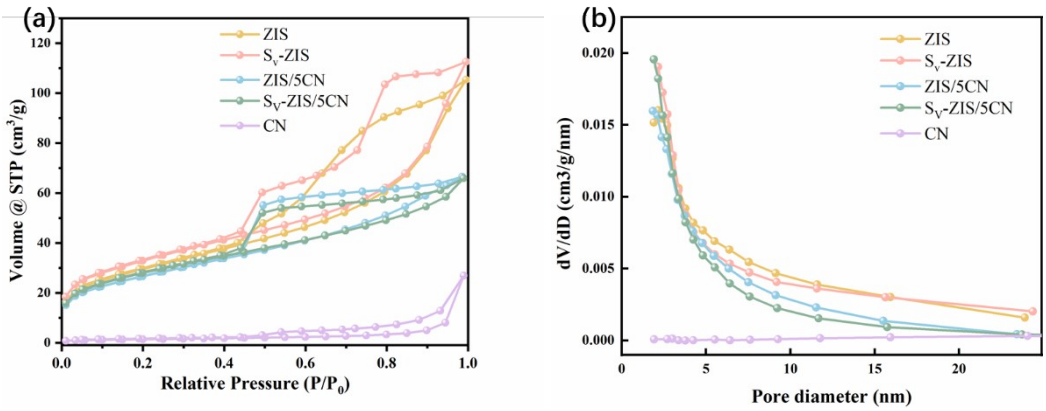

Fig. S2 (a) N_2 adsorption–desorption isotherms and (b) pore size distributions results of CN, ZIS, ZIS/5CN, S_V-ZIS and S_V-ZIS/5CN composite.

Table S1. BET surface area and average pore diameters of ZIS, S_V-ZIS, ZIS/5CN, S_V-ZIS/5CN and CN.

Sample	Surface area (m^2g^{-1})	Average pore diameter (nm)
ZIS	105.6916	5.4702
S_v-ZIS	118.2983	5.4230
ZIS/5CN	95.6263	4.0761
S_v-ZIS/5CN	101.0246	4.0883
CN	5.3236	14.2949

3. XPS spectra of as-prepared samples

The full-band spectra of all the samples are shown in Fig. S3a, the CN monomer consists of C 1s and N 1s spectral signature signals, and the S_V-ZIS monomer consists of Zn 2p, In 3d, and S 2p spectral signature signals. The elemental signature peaks of the S_V-ZIS/CN corresponded to the two pure semiconductors, which proved that the two semiconductors were successfully composited together. Two peaks (1022.77 and 1045.91 eV) were divided in the Zn 2p spectra of ZIS in Fig. S3a, classifying as Zn $2p_{3/2}$ and Zn $2p_{1/2}$[5], respectively. The In 3d spectrum of ZIS (Fig. S3b) reveals deconvoluted In $3d_{5/2}$ and In $3d_{3/2}$ peaks centered at 445.28 and 4552.87 eV[6].

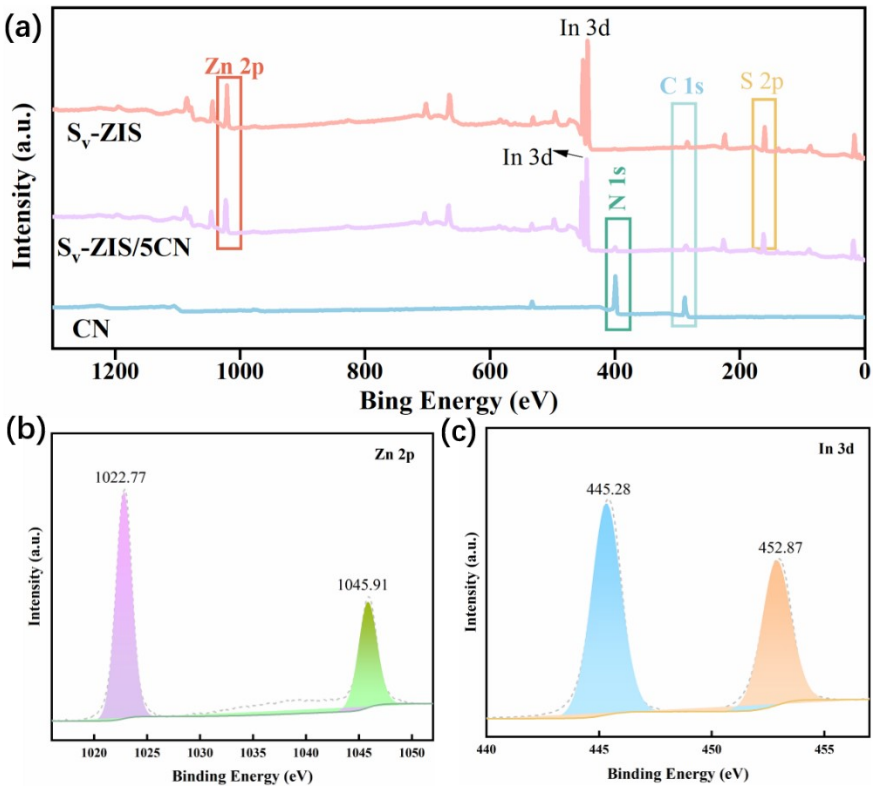

Fig. S3 (a) Typical XPS survey spectra of CN, S_V-ZIS and S_V-ZIS/5CN heterojunction, high-resolution XPS of (b) Zn 2p and (c) In 3d of ZIS.

4. Optical property and band structure of ZIS

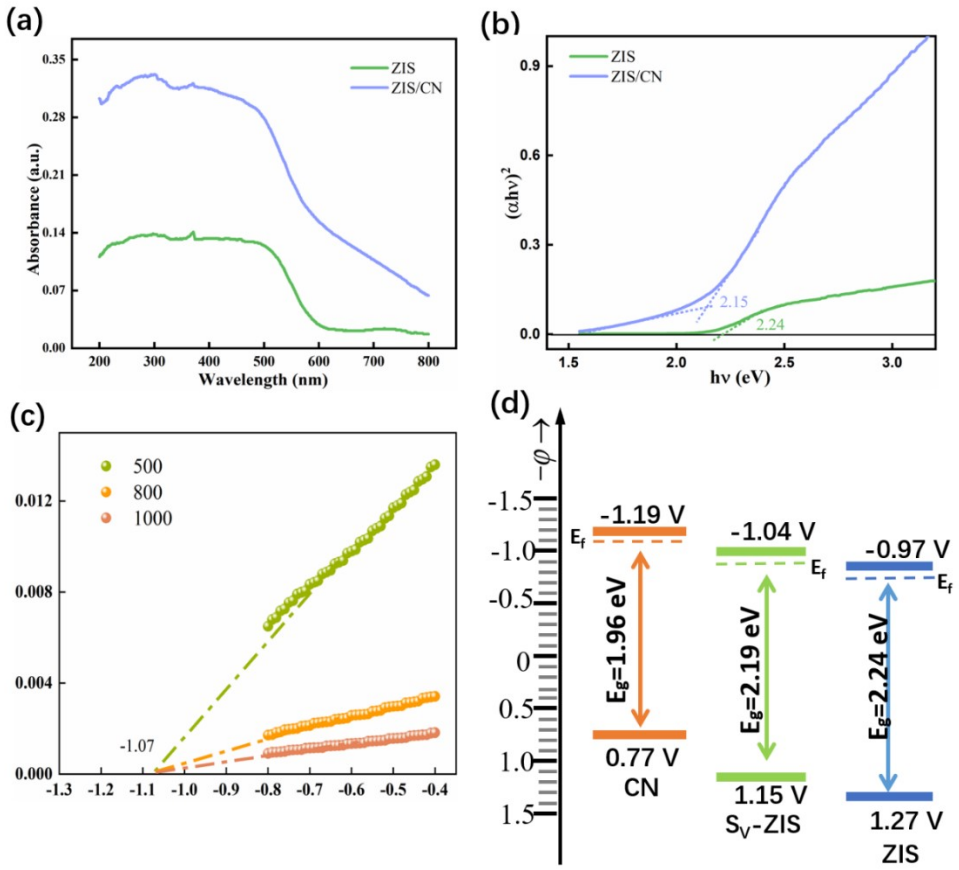

Fig. S4 (a) DRS and (b) Eg of ZIS and ZIS/CN. (c) M-S plots of ZIS, (d) band structures of CN, S_V-ZIS and ZIS.

5.VB-XPS of CN and S_V-ZIS

The experimental VB positions of CN (1.0 eV) and S_V-ZIS (1.37 eV) are obtained from the XPS valence band spectra. The actual values of CN (0.78 V) and S_V-ZIS (1.15 V) are calculated by using $E_{NHE}/V = \varphi + f - 4.44$ (E_{NHE}: the potential of the normal hydrogen electrode; φ: Instrumental work function (φ = 4.2 eV); f: the test value of VB spectra)[7].

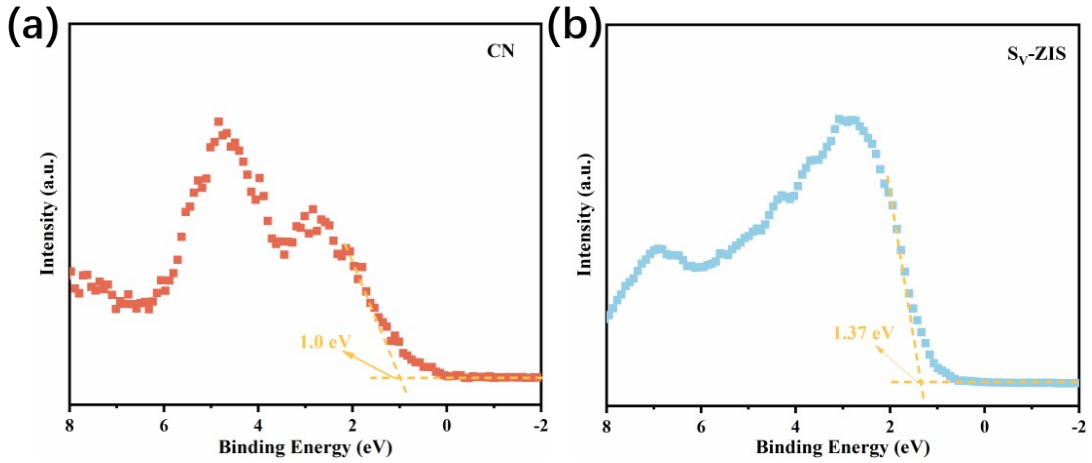

Fig. S5 VB XPS spectra of (a) CN and (b) S_V-ZIS.

6. PDOS of CN, ZIS and S_V-ZIS

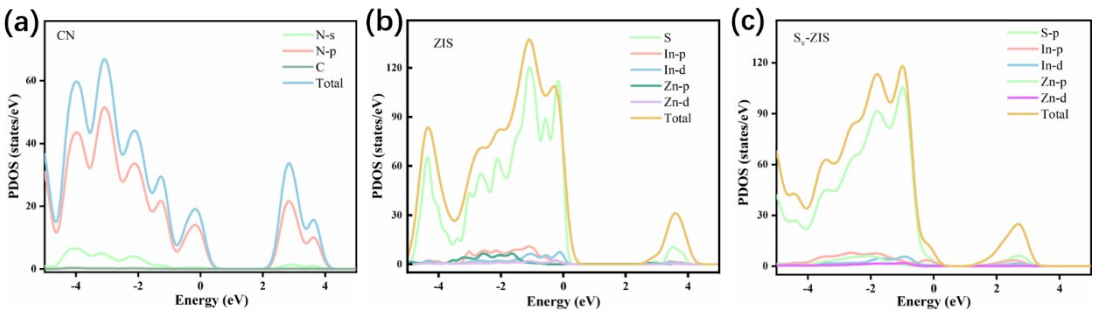

Fig. S6 DOS distribution maps of CN, ZIS and S_V-ZIS.

7. Photo-deposition experiment

To visually illustrate the spatial separation and migration paths of photogenerated carriers, a selective photodeposition experiment was conducted. This method utilized the fact that Mn^{2+} can be oxidized by photogenerated holes to form insoluble MnO_X species, while Ag^+ can be reduced by photogenerated electrons to generate metal Ag nanoparticles, thereby marking the locations of hole and electron accumulation respectively.

For the photo-deposition of Ag nanoparticles (electron tracer): 20 mg of S_V-ZIS/CN photocatalyst was dispersed in 50 mL of methanol-water solution (10 vol%) and an appropriate amount of $AgNO_3$ was added to achieve a nominal 5 wt% Ag loading. The mixture was stirred magnetically in the dark for 30 min to establish an adsorption-desorption equilibrium, and then continuously stirred under visible light irradiation ($\lambda > 420$ nm) for 1 h to drive the reduction process.

For the photo-deposition of MnO_X (hole tracer): 20 mg of S_V-ZIS/CN photocatalyst was suspended in 50 mL of water solution containing $MnCl_2$ (0.1 mg/mL) and KIO_3 (0.4 mM). After stirring in the dark for 30 min, the mixture was placed under visible light irradiation for 2 h. After the irradiation, all the products were collected by centrifugation, thoroughly washed with deionized water, and dried for subsequent microscopic analysis to determine the deposition location.

The charge migration pathways during the photocatalytic process were further verified by selectively depositing the metals Ag and MnO_X. Under light conditions, when Ag was deposited alone, it could be observed that Ag particles were deposited on the CN surface (Fig. S7a). This indicates that the photogenerated electrons are more likely to exist on the CN surface, meaning that the reduction sites are located on the CN surface. Furthermore, it was found that the MnOX nanosheets were deposited on the surface of S_V-ZIS (Fig. S7b), indicating that photogenerated holes gathered on the surface of S_V-ZIS. Therefore, there were oxidation sites on the S_V-ZIS surface that participated in the oxidation reaction. The optical deposition experiment further confirmed the existence of the S-scheme heterojunction.

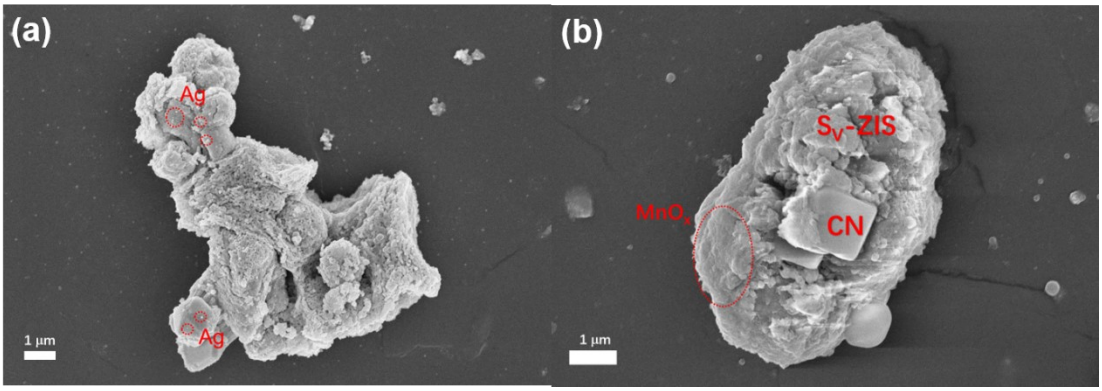

Fig. S7 SEM image after the experiments of depositing (a) Ag and (b) MnO_X by photo-deposition on the S_V-ZIS/CN.

8. Wavelength-dependent apparent quantum efficiency for ZIS/5CN

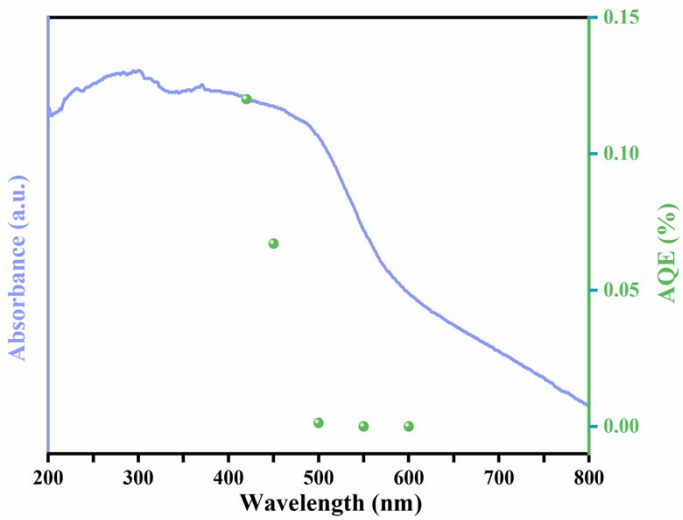

Fig. S8. Wavelength-dependent apparent quantum efficiency of ZIS/5CN composite.

9. XRD, SEM and HRTEM image of the S_V-ZIS/5CN catalyst after the cycle

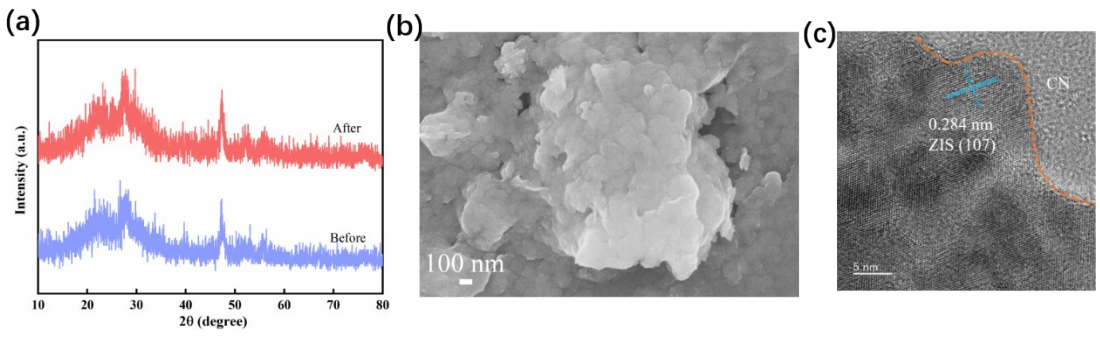

Fig. S9. (a) XRD, (b) SEM and (c) TEM image of the S_V-ZIS/5CN catalyst after the four-cycle.

10. surface potential distribution and PL spectra of the samples

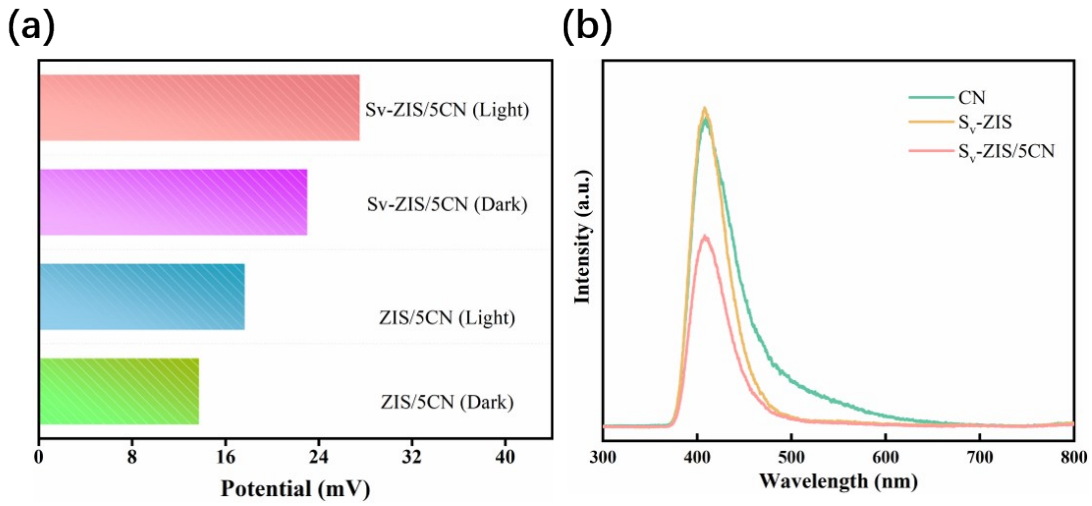

Fig. S10. (a) The surface potentials of ZIS/5CN and S_V-ZIS/5CN under dark and light conditions. (b) PL spectra of CN, S_V-ZIS and S_V-ZIS/5CN catalyst.

11. AQE data

Table S2. AQE data.

Wavelength (nm)	Light intensity (W)	H_2 evolution rate (mmol/g/h)	AQE (%)
420	0.142	2.92388	7.45
450	0.140	1.01212	2.41
500	0.136	0.5009	1.07
550	0.133	0.1339	0.26
600	0.127	0	0
650	0.121	0	0

Table S3. Comparison of AQEs with previously reported $ZnIn_2S_4$-based semiconductor photocatalysts.

Photocatalyst	Wavelength (nm)	Light intensity (mW cm^{-2})	AQE (%)	Ref.
S_V-$ZnIn_2S_4$/C_3N_5	420	45.2	7.45	This work
$ZnIn_2S_4$/MOF	365	5.1	2.57	[8]
S_V-$ZnIn_2S_4$	420	86.82	0.16	[9]
$ZnIn_2S_4$/CdS	420	44.76	12.6	[10]
MoS_2/O-$ZnIn_2S_4$	420	70	~2.53	[11]
$ZnMoO_4$@ $ZnIn_2S_4$	420	/	8.32	[12]
N-CeO_2-δ@$ZnIn_2S_4$	420	/	15.9	[13]
TiO_2–$ZnIn_2S_4$	420	19.75	1.1	[14]
$BiVO_4$@$ZnIn_2S_4$/Ti_3C_2	410	/	2.4	[15]
$ZnIn_2S_4$/$NiWO_4$	420	10.1	9.69	[16]
S-g-C_3N_4/$ZnIn_2S_4$	420	/	34.43	[17]

12. Comparison of the H_2 evolution efficiency

Table S4. Comparison of the hydrogen evolution efficiency of representative C_3N_5 and $ZnIn_2S_4$-based photocatalysts.

Photocatalyst	Sacrificial agent	Cocatalyst/ sensitizer	Light source	Activity (mmol h^{-1} g^{-1})	Reference
$ZnIn_2S_4$/ C_3N_5	10 vol% TEOA	1 wt% Pt	300 W Xe lamp (>420 nm)	4.85	This work
C_3N_4/rGO/C_3N_5	10 vol% TEOA	/	300 W Xe lamp (>400 nm)	0.32	[18]
V_2O_5/C_3N_5	10 vol% TEOA	0.2 wt% Pt	300 W Xe lamp (>420 nm)	0.33	[19]
$CoFe_2O_4$/$ZnIn_2S$	20 vol% TEOA	3 wt% Pt	300 W Xe lamp	0.80	[20]

4			(>420 nm)		
C_3N_5/TiO_2	10 vol% TEOA	/	300 W Xe lamp (>420 nm)	1.83	21
BDCNN/$ZnIn_2S_4$	10 vol% TEOA	1 wt% Pt	300 W Xe lamp (>420 nm)	2.38	22
C_3N_5/Ti_3C_2	10 vol% TEOA	1 wt% Pt	300 W Xe lamp (>420 nm)	2.59	23
$BiVO_4/C_3N_5$	0.4 g sodium ascorbate	1 wt% Pt	300 W Xe lamp (>420 nm)	2.62	24
$SnIn_4S_8/ZnIn_2S_4$	10 vol% TEOA	3 wt% Pt	300 W Xe lamp (>420 nm)	2.99	25
$ZnIn_2S_4$/ZnSe	0.25 M Na_2SO_3 and 0.35 M Na_2S	1 wt% Pt	300 W Xe lamp (>420 nm)	3.33	6
C_3N_4/C_3N_5	10 vol% TEOA	1 wt% Pt	300 W Xe lamp (>420 nm)	3.33	26
$ZnIn_2S_4$/MXene	10 vol% TEOA	3 wt% Pt	300 W Xe lamp (>420 nm)	3.48	27
$ZnIn_2S_4$/CPCN	0.25 M Na_2SO_3 and 0.35 M Na_2S	/	300 W Xe lamp (>420 nm)	3.49	28
MoS_2/O-$ZnIn_2S_4$	0.25 M Na_2SO_3 and 0.35 M Na_2S	/	300 W Xe lamp	4.01	29
$ZnWO_4/ZnIn_2S_4$	5 vol% methanol		300 W Xe lamp (>420 nm)	4.93	30
$ZnIn_2S_4/BiVO_4$	10 vol% TEOA	3 wt% Pt	300 W Xe lamp (>400 nm)	5.90	31
S-$C_3N_4/ZnIn_2S_4$	0.25 M Na_2SO_3 and 0.35 M Na_2S	/	300 W Xe lamp (>420 nm)	8.46	32

13.Summary of the fitting parameters for the TR-PL decay curves

Table S5. Lifetime parameters of S_V-ZIS, ZIS/5CN and S_V-ZIS/5CN from the TRPL results.

Sample	A_1 [%]	A_2 [%]	τ_1 [ns]	τ_2 [ns]	τ_A [ns]
S_v-ZIS	994.005	46.564	1.13	12.42	4.96726
ZIS/5CN	891.792	123.125	1.786	10.9	5.95376
S_v-ZIS/5CN	1075.801	68.436	1.006	16.96	9.2619

The average lifetime was calculated by using the **Equation**:

$$\tau_{\text{Ave.}} = \frac{A_1 \cdot \tau_1^2 + A_2 \cdot \tau_2^2}{A_1 \cdot \tau_1 + A_2 \cdot \tau_2}$$

References

1 A. Raja, N. Son, M. Swaminathan and M. Kang, *J. Colloid. Interface. Sci.*, 2021, **602**, 669-679.

2 H. Che, J. Wang, X. Gao, J. Chen, P. Wang, B. Liu and Y. Ao, *J. Colloid. Interface. Sci.*, 2022, **627**, 739-748.

3 J. Cai, B. Liu, S. Zhang, L. Wang, Z. Wu, J. Zhang and B. Cheng, *J. Mater. Sci. Technol.*, 2024, **197**, 183-193.

4 Q. Liang, W. Gao, C. Liu, S. Xu and Z. Li, *J. Hazard. Mater.*, 2020, **392**.

5 X. Lian, Z. Huang, Y. Zhang, Z. Chen, P. Meidl, X. Yi and B. Xu, *Chemosphere*, 2023, **313**, 137351.

6 Y. Zhong, M. Li, X. Luan, F. Gao, H. Wu, J. Zi and Z. Lian, *Applied Catalysis B: Environmental*, 2023, **335**, 122859.

7 N. Tian, H. Huang, S. Wang, T. Zhang, X. Du and Y. Zhang, *Applied Catalysis B: Environmental*, 2020, **267**, 118697.

8 J. Cai, B. Liu, S. Zhang, L. Wang, Z. Wu, J. Zhang and B. Cheng, *J. Mater. Sci. Technol.*, 2024, **197**, 183-193.

9 X. Jing, N. Lu, J. Huang, P. Zhang and Z. Zhang, *J. Energy Chem.*, 2021, **58**, 397-407.

10 C. Li, X. Du, S. Jiang, Y. Liu, Z. Niu, Z. Liu, S. Yi and X. Yue, *Adv. Sci.*, 2022, **9**, 2201773.

11 Y. Peng, X. Guo, S. Xu, Y. Guo, D. Zhang, M. Wang, G. Wei, X. Yang, Z. Li, Y. Zhang and F. Tian, *J. Energy Chem.*, 2022, **75**, 276-284.

12 S. Wang, Q. Liu, W. Zhang, J. Liu, X. Ji, P. Cai, R. Chen, S. Liu, W. Ma, D. Zhang and X. Pu, *Carbon Neutralization*, 2025, **4**, e70054.

13 S. Farhan, A. Hassan Raza, S. Yang, Z. Yu and Y. Wu, *J. Colloid. Interface. Sci.*, 2024, **669**, 430-443.

14 G. Zuo, Y. Wang, W. L. Teo, Q. Xian and Y. Zhao, *Applied Catalysis B: Environmental*, 2021, **291**, 120126.

15 X. Du, T. Zhao, Z. Xiu, Z. Xing, Z. Li, K. Pan, S. Yang and W. Zhou, *Appl. Mater. Today*, 2020, **20**, 100719.

16 H. Lv, H. Wu, J. Zheng, Y. Kong, X. Xing, G. Wang and Y. Liu, *Colloids and Surfaces a:*

Physicochemical and Engineering Aspects, 2023, **666**, 131384.
17 T. Wang, X. Pan, M. He, L. Kang and W. Ma, *Adv. Sci.*, 2024, **11**, 2403771.
18 D. Liu, J. Yao, S. Chen, J. Zhang, R. Li and T. Peng, *Applied Catalysis B: Environmental*, 2022, **318**, 121822.
19 F. Liu, Q. Zhang, C. Chen, Z. Zhang and X. Fang, *Sol. Energy Mater. Sol. Cells*, 2023, **257**, 112385.
20 C. Li, H. Che, P. Huo, Y. Yan, C. Liu and H. Dong, *J. Colloid. Interface. Sci.*, 2021, **581**, 764-773.
21 S. Chen, X. Sheng, Y. Wang, P. Yu, C. Yang, X. Zhang, H. Fang, Y. Zhang and Y. Zhou, *Appl. Surf. Sci.*, 2024, **643**, 158600.
22 J. Liu, Y. Fu, G. Chu, K. Wen, L. Qiu, P. Li, L. Cheng, B. Cao, Y. Tang, X. Chen, H. Kita and S. Duo, *Process Saf. Environ. Protect.*, 2024, **191**, 883-896.
23 P. Yu, S. Chen, Y. Wang, J. Li, Z. Zhang, S. Zhao, Y. Zhang and Y. Zhou, *Int. J. Hydrog. Energy*, 2024, **58**, 1266-1276.
24 W. Wang, B. Li, J. Shi, K. Zhu, Y. Zhang, X. Liu, C. Li, F. Hu, X. Xi and S. Kawi, *Applied Catalysis B: Environment and Energy*, 2025, **362**, 124766.
25 R. Xiong, C. Tang, S. Liu, Y. Xiao, B. Cheng and S. Lei, *Sep. Purif. Technol.*, 2022, **295**, 121267.
26 N. Su, S. Cheng, P. Zhang, H. Dong, Y. Fang, X. Zhou, Y. Wang and C. Li, *Int. J. Hydrog. Energy*, 2022, **47**, 41010-41020.
27 G. Zuo, Y. Wang, W. L. Teo, A. Xie, Y. Guo, Y. Dai, W. Zhou, D. Jana, Q. Xian, W. Dong and Y. Zhao, *Angewandte Chemie International Edition*, 2020, **59**, 11287-11292.
28 C. Zhang, L. Lin, M. Zhou, Y. Wang, S. Xu, X. Chen and Z. Li, *Chem. Eng. J.*, 2024, **495**, 153563.
29 Y. Peng, X. Guo, S. Xu, Y. Guo, D. Zhang, M. Wang, G. Wei, X. Yang, Z. Li, Y. Zhang and F. Tian, *J. Energy Chem.*, 2022, **75**, 276-284.
30 M. Dai, Z. He, P. Zhang, X. Li and S. Wang, *J. Mater. Sci. Technol.*, 2022, **122**, 231-242.
31 J. Hu, C. Chen, Y. Zheng, G. Zhang, C. Guo and C. M. Li, *Small*, 2020, **16**, 2002988.
32 T. Wang, X. Pan, M. He, L. Kang and W. Ma, *Adv. Sci.*, 2024, **11**, 2403771.